

EFFECTS OF TRIAXIALITY ON THE STATISTICS OF LARGE-SEPARATION GRAVITATIONAL LENSES

MASAMUNE OGURI¹ AND CHARLES R. KEETON^{2,3}

accepted by ApJ

ABSTRACT

We study the statistics of large-separation gravitational lens systems produced by non-spherical halos in the Cold Dark Matter (CDM) model. Specifically, we examine how the triaxiality of CDM halos affects the overall lensing probabilities and the relative numbers of different image configurations (double, quadruple, and naked cusp lenses). We find that triaxiality significantly enhances lensing probabilities by a factor of ~ 2 – 4 , so it cannot be ignored. If CDM halos have central density slopes $\alpha \lesssim 1.5$, we predict that a significant fraction ($\gtrsim 20\%$) of large-separation lenses should have naked cusp image configurations; this contrasts with lensing by isothermal ($\alpha \approx 2$) galaxies where naked cusp configurations are rare. The image multiplicities depend strongly on the inner density slope α : for $\alpha = 1$, the naked cusp fraction is $\gtrsim 60\%$; while for $\alpha = 1.5$, quadruple lenses are actually the most probable. Thus, the image multiplicities in large-separation lenses offer a simple new probe of the inner density profiles of dark matter halos. We also compute the expected probabilities and image multiplicities for lensed quasars in the Sloan Digital Sky Survey, and argue that the recent discovery of the large-separation quadruple lens SDSS J1004+4112 is consistent with expectations for CDM.

Subject headings: cosmology: theory — dark matter — galaxies: clusters: general — gravitational lensing

1. INTRODUCTION

The Cold Dark Matter (CDM) model of structure formation naturally predicts the existence of strong gravitational lens systems with image separations of $\sim 10''$ or even larger. Observations of massive clusters of galaxies have revealed many systems of “giant arcs” representing lensed images of background galaxies (Lynds & Petrosian 1986; Soucail et al. 1987; Luppino et al. 1999; Gladders et al. 2003; Zaritsky & Gonzalez 2003). However, until recently all lensed quasars and radio sources had image separations $< 7''$ corresponding to lensing by galaxies, despite some explicit searches for lenses with larger separations (Phillips et al. 2001; Ofek et al. 2001).⁴ Lensing of quasars by clusters was finally observed with the recent discovery and confirmation of SDSS J1004+4112, a quadruple lens with an image separation of $14''.62$ found in the Sloan Digital Sky Survey (Inada et al. 2003; Oguri et al. 2004). This lens confirms an important prediction of the CDM model; indeed, the lensing probability inferred from the discovery is in agreement with reasonable values of the cosmological parameters (Oguri et al. 2004).

The statistics of large-separation lenses can be used to place constraints on the density profile of dark halos (Maoz et al. 1997; Keeton & Madau 2001; Keeton 2001a; Wyithe, Turner, & Spergel 2001; Takahashi &

Chiba 2001; Sarbu, Rusin, & Ma 2001; Li & Ostriker 2002; Oguri et al. 2002; Oguri 2002; Huterer & Ma 2004; Kuhlen, Keeton, & Madau 2004), or determine the abundance of massive dark halos (Narayan & White 1988; Wambsganss et al. 1995; Kochanek 1995; Nakamura & Suto 1997; Mortlock & Webster 2000; Oguri 2003; Lopes & Miller 2004; Chen 2004). The discovery of the first such lens suggests that these statistics can be a practical tool to study structure formation in the universe. The statistics of giant arcs are also known as a good probe of clusters (Bartelmann et al. 1998; Meneghetti et al. 2001; Molikawa & Hattori 2001; Oguri, Taruya, & Suto 2001; Oguri, Lee, & Suto 2003; Wambsganss, Bode, & Ostriker 2004; Dalal, Holder, & Hennawi 2004; Macciò 2004), and in fact lensed arcs and quasars complement each other in several ways. For instance, in lensed quasar surveys one first identifies source quasars and then checks whether they are lensed, while in searching for lensed arcs one selects massive clusters and then searches for lensed arcs in them. In other words, surveys for arcs are biased toward high mass concentrations, while lensed quasars probe random lines of sight. Clusters selected by the presence of lensed quasars could, in principle, differ from those selected as having giant arcs. In addition, lensed quasars have three advantages over lensed arcs in statistical studies. First, quasars can be regarded as point sources, while sources for arcs are galaxies whose intrinsic sizes and shapes are important but unobservable. Second, the number and configuration of images in a quasar lens system is unambiguous. Third, the redshift distribution of arc sources is poorly known (and controversial; see Oguri et al. 2003; Wambsganss et al. 2004; Dalal et al. 2004), while the redshift distribution of quasars is well known.

In all previous analytic work on the statistics of large-separation lensed quasars, the lens objects were assumed to be spherical. However, in the CDM model dark halos are not spherical at all but triaxial (e.g. Jing & Suto

¹ Department of Physics, University of Tokyo, Hongo 7-3-1, Bunkyo-ku, Tokyo 113-0033, Japan.

² Astronomy and Astrophysics Department, University of Chicago, 5640 South Ellis Avenue, Chicago, IL 60637 USA.

³ Hubble Fellow

Electronic address: oguri@utap.phys.s.u-tokyo.ac.jp (MO), ckeeton@oddjob.uchicago.edu (CRK)

⁴ Miller et al. (2004) recently reported six pairs of quasars in the Two-Degree Field (2dF) Quasar Redshift Survey that are candidate lenses with image separations on the scale of an arcminute; but none of the candidates has been confirmed, and theoretical arguments by Oguri (2003) indicate that it would be quite surprising if any of the systems are lenses.

2002, hereafter JS02). It is already known that triaxiality has a significant effect on the statistics of lensed arcs, from both analytic (Oguri et al. 2003, hereafter OLS03) and numerical (Meneghetti, Bartelmann, & Moscardini 2003a; Dalal et al. 2004) points of view. In the statistics of normal lensed quasars, triaxiality (or ellipticity) has been thought to mainly affect the image multiplicities, with only small changes to the total lensing probability (Kochanek 1996; Keeton, Kochanek, & Seljak 1997; Evans & Hunter 2002; Chae 2003; Huterer & Keeton 2004). However, that conclusion is based on nearly-singular isothermal lens models, and the situation may be quite different for the less concentrated mass distributions of the massive halos that create large-separation lenses. Moreover, only triaxial modeling allows us to study image multiplicities, and to consider whether it is statistically natural that the first known large-separation lens is a quadruple.

The structure of this paper is as follows. In §2 we review the triaxial dark halo model and its lensing properties (originally presented by JS02 and OLS03). In §3 we show our general results, while in §4 we customize our predictions to the SDSS quasar sample. We summarize our conclusions in §5. Throughout the paper, we assume a Λ -dominated cosmology with current matter density $\Omega_M = 0.3$, cosmological constant $\Omega_\Lambda = 0.7$, dimensionless Hubble constant $h = 0.7$, and normalization of matter density fluctuations $\sigma_8 = 0.9$.

2. FORMALISM

2.1. Lensing by triaxial dark halos

In this section, we briefly summarize the lensing properties of the triaxial model of dark halos proposed by JS02. For more details, please refer to JS02 and OLS03.

First, we relate the principal coordinate system of the triaxial dark halo $\vec{x} = (x, y, z)$ to the observer's coordinate system $\vec{x}' = (x', y', z')$, where the z' -axis runs along the line of sight to the observer. In general, the coordinate transformation is expressed as $\vec{x} = A\vec{x}'$ with

$$A \equiv \begin{pmatrix} -\sin\phi & -\cos\phi\cos\theta & \cos\phi\sin\theta \\ \cos\phi & -\sin\phi\cos\theta & \sin\phi\sin\theta \\ 0 & \sin\theta & \cos\theta \end{pmatrix}. \quad (1)$$

The density profiles of triaxial dark matter halos proposed by JS02 (also see Zhao 1996) is

$$\rho(R) = \frac{\delta_{ce}\rho_{\text{crit}}(z)}{(R/R_0)^\alpha(1+R/R_0)^{3-\alpha}}, \quad (2)$$

where

$$R^2 \equiv c^2 \left(\frac{x^2}{a^2} + \frac{y^2}{b^2} + \frac{z^2}{c^2} \right) \quad (a \leq b \leq c). \quad (3)$$

Two models commonly discussed in the context of CDM simulations are $\alpha = 1$ and 1.5 (Navarro, Frenk, & White 1997; Fukushige & Makino 1997; Moore et al. 1999; Jing & Suto 2000; Power et al. 2003; Fukushige, Kawai, & Makino 2004), and we focus on these. JS02 give fitting formulas for the axis ratios a/c and a/b in the triaxial model, and for the concentration parameter $c_e \equiv R_e/R_0$, where R_e is defined such that the mean density within the ellipsoid of the major axis radius R_e is $\Delta_e\Omega(z)\rho_{\text{crit}}(z)$ with $\Delta_e = 5\Delta_{\text{vir}}(c^2/ab)^{0.75}$.

What matters for lensing is the projected surface mass density in units of the critical density for lensing, or the convergence κ , which can be expressed as (OLS03)

$$\kappa = \frac{b_{\text{TNFW}}}{2} f_{\text{GNFW}} \left(\frac{1}{R_0} \sqrt{\frac{(x')^2}{q_x^2} + \frac{(y')^2}{q_y^2}} \right), \quad (4)$$

where b_{TNFW} is a dimensionless “strength” parameter (defined in OLS03), $q \equiv q_y/q_x \leq 1$ is the axis ratio of the projected mass distribution, and

$$f_{\text{GNFW}}(r) \equiv \int_0^\infty \frac{1}{(\sqrt{r^2+z^2})^\alpha (1+\sqrt{r^2+z^2})^{3-\alpha}} dz. \quad (5)$$

For $\alpha = 1$, equation (5) has an analytic expression (Bartelmann 1996). For $\alpha = 1.5$, we adopt a fitting formula for equation (5) presented by OLS03. Note that the convergence has elliptical symmetry, so the lensing deflection and magnification can be computed with a set of 1-dimensional integrals (Schramm 1990; Keeton 2001b). Also note that if we work in dimensionless units, scaling all lengths by $L_0 \equiv R_0q_x$, then the lensing properties of the dark matter halos depend only on the parameters α , b_{TNFW} , and q .

2.2. Cross sections and image separation distributions

We compute lensing cross sections using Monte Carlo methods. Working in dimensionless coordinates $X \equiv x'/L_0$ and $Y \equiv y'/L_0$, we pick random sources and use the *gravlens* software by Keeton (2001b) to solve the lens equation. Figure 1 shows examples of the three different kinds of image configurations: double, quadruple, and naked cusp lenses.⁵ We count the number of sources that produce lenses of different image multiplicities to determine the dimensionless cross sections $\tilde{\sigma}_2$, $\tilde{\sigma}_4$, and $\tilde{\sigma}_c$ for doubles, quadruples, and cusps, respectively. For each set of images, we define the dimensionless image separation $\tilde{\theta}$ to be the maximum separation between any pair of images; this is a convenient definition that depends only on observable quantities and is well defined for all image configurations (no matter how many images there are). We bin the sources by the image separations they produce to derive image separation distributions, as shown in Figures 2 and 3. For a given halo there is a range of separations, but it tends to be fairly narrow ($\lesssim 20\%$); the main exception is for cusp configurations, which show a tail to small separations that corresponds to sources near the cusp in the caustic.

If we not only count the sources but also weight them appropriately, we can compute the magnification bias. Specifically, if the sources have a simple power law luminosity function $\phi_L(L) \propto L^{-\beta}$ then the “biased cross section” can be written as

$$B\tilde{\sigma} = \int dXdY \frac{\phi_L(L/\mu)/\mu}{\phi_L(L)} = \int dXdY \mu^{\beta-1}, \quad (6)$$

where the integral is over the multiply-imaged region of the source plane. We can compute the biased cross sections for doubles, quadruples, and cusps similarly. Each

⁵ We use the terms “double” and “quadruple” because the third and fifth images are usually too faint to be observed, although with the density profiles we use here they are probably not as faint as for nearly-isothermal lenses (see Rusin 2002).

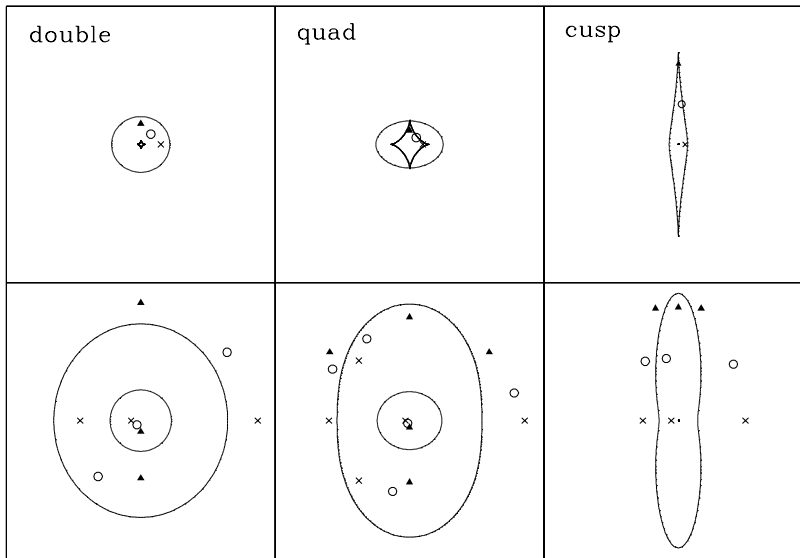


FIG. 1.— Sample image configurations. The top panels show the source planes, and the bottom panels show the corresponding image planes. The solid lines indicate the caustics and critical curves. We show three sources (denoted by triangles, circles, crosses), and their corresponding images. From left to right, the lenses are doubles, quadruples, and cusps. Specific values of (b_{TNGFW}, q) for each example are $(2, 0.95)$, $(2, 0.75)$, and $(0.6, 0.25)$ for doubles, quadruples, and cusps, respectively. Doubles and cusps are distinguished by the image parities: doubles have one positive-parity image and one negative-parity image, plus a central double-negative image that is usually too faint to be observed; while cusps have two positive-parity images and one negative parity image, all of comparable brightnesses.

source is to be weighted by $\mu^{\beta-1}$, where we take μ to be the magnification of the second brightest image to reflect the method of searching for large-separation lenses in observational data such as the SDSS (see Inada et al. 2003; Oguri et al. 2004).

An important qualitative result is already apparent from Figure 1. CDM-type dark matter halos are very sensitive to departures from spherical symmetry, in the sense that even small projected ellipticities lead to large tangential caustics and hence large quadruple cross sections. When the ellipticity is large, the tangential caustic is much larger than the radial caustic and nearly all the images correspond to cusp configurations. This situation is notably different from what happens in lensing by galaxies that have concentrated, roughly isothermal mass distributions. In that case, the ellipticity must approach unity before cusp configurations become common (see Keeton et al. 1997; Rusin & Tegmark 2001). Such large ellipticities are uncommon, and cusp configurations are correspondingly rare among observed galaxy-scale lenses: among ~ 80 known lenses there is only one candidate (APM 08279+5255; Lewis et al. 2002). The incidence of cusp configurations therefore appears to be a significant distinction between normal and large-separation lenses.

2.3. Lensing probabilities

The probability that a source at redshift z_S is lensed into a system with image separation θ is computed by summing the biased cross section over an appropriate population of lens halos:

$$\frac{dP}{d\theta}(\theta, z_S) = \int dz_L \frac{c dt}{dz_L} (1 + z_L)^3 \int d(a/c) \int dc_e \\ \times \int d(a/b) \int d\theta \int d\phi \left[p(a/c) p(c_e) \right]$$

$$p(a/b|a/c) p(\theta) p(\phi) B\sigma \frac{dn}{dM} \Big]_{M(\theta)}. \quad (7)$$

The first integral is over the volume between the observer and the source. The next three integrals are over the structural parameters of the lens halos, while the last two integrals cover the different orientations. The mass function of dark matter halos is dn/dM , and we use the model from equation (B3) of Jenkins et al. (2001). Finally, $M(\theta)$ is the mass of a halo that produces image separation θ (for given redshift and other parameters), which is given by the solution of

$$\theta = R_0 q_x \tilde{\theta}(b_{\text{TNGFW}}, q). \quad (8)$$

The square brackets in equation (7) indicate that the integrand is to be evaluated only for parameter sets that produce the desired image separation. Equation (7) gives the total lensing probability, but we can simply replace the total biased cross section $B\sigma$ with $B_2\sigma_2$, $B_4\sigma_4$, or $B_c\sigma_c$ to compute the probability for doubles, quadruples, or cusps.

We use the model given by JS02 for the probability distribution functions (PDFs) that appear in equation (7). The PDFs for the axis ratios are:

$$p(a/c) = \frac{1}{\sqrt{2\pi} \times 0.113} \\ \times \exp \left[-\frac{\left\{ (a/c)(M_{\text{vir}}/M_*)^{0.07[\Omega(z)]^{0.7}} - 0.54 \right\}^2}{2(0.113)^2} \right] \\ \times \left(\frac{M_{\text{vir}}}{M_*} \right)^{0.07[\Omega(z)]^{0.7}}, \quad (9)$$

$$p(a/b|a/c) = \frac{3}{2(1 - \max(a/c, 0.5))}$$

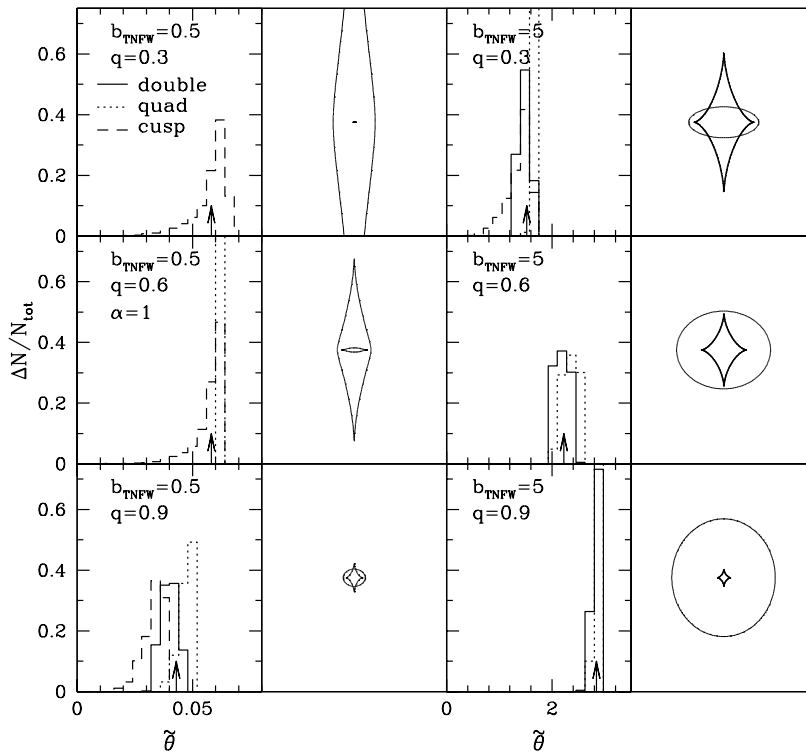


FIG. 2.— Image separation distributions for sample lenses with $\alpha = 1$. Arrows indicate the average separations. The corresponding caustics are shown for reference. For each b_{TNFW} , the caustics are all plotted on the same scale.

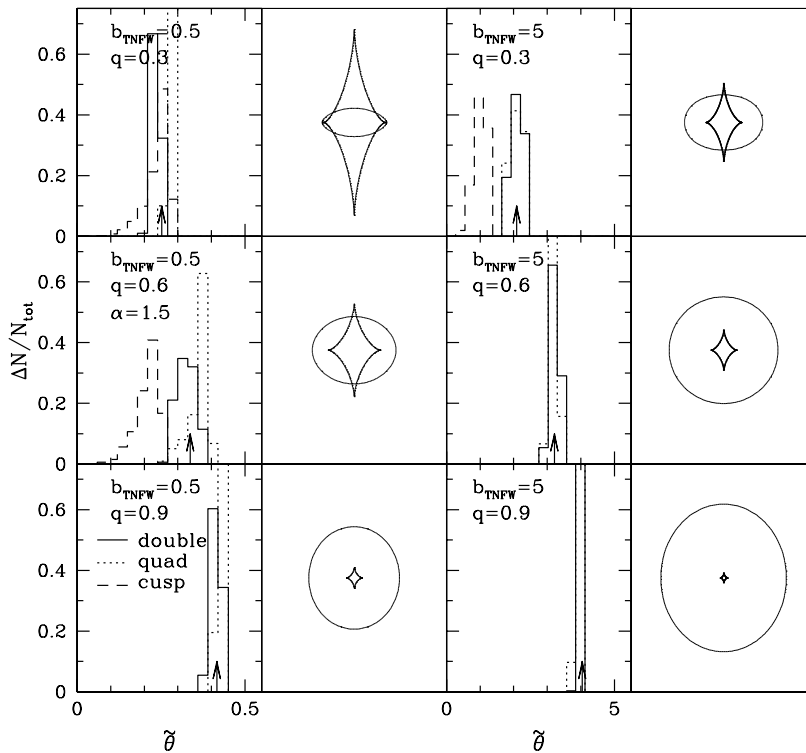


FIG. 3.— Similar to Figure 2, but for $\alpha = 1.5$.

$$\times \left[1 - \left(\frac{2a/b - 1 - \max(a/c, 0.5)}{1 - \max(a/c, 0.5)} \right)^2 \right], \quad (10)$$

where M_* is the characteristic nonlinear mass such that

the RMS top-hat-smoothed overdensity at that mass scale is 1.68. Note that M_* and $\Omega(z)$ depend on redshift, so $p(a/c)$ varies with redshift such that halos tend to be more triaxial at higher redshifts (see Fig. 8 of JS02).

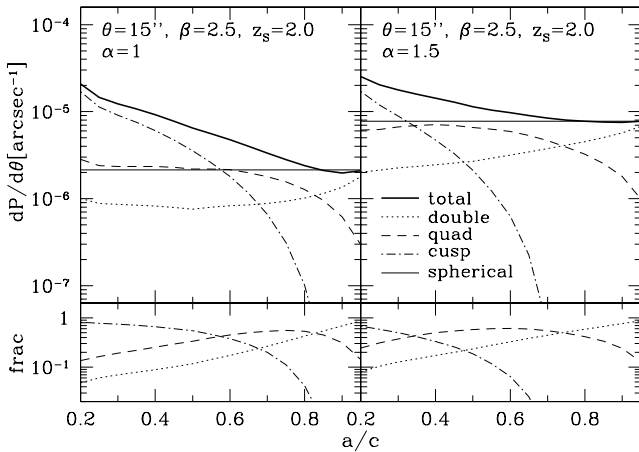


FIG. 4.— Lensing probabilities and image multiplicities as a function of a/c . The left panels are for inner slope $\alpha = 1$, and the right panels for $\alpha = 1.5$. We adopt $\theta = 15''$, $\beta = 2.5$, and $z_s = 2.0$. We show the total lensing probability (thick solid line), as well as the probabilities for double (dotted), quadruple (dashed), and cusp (dash-dotted) lenses. For comparison, the lensing probability of spherical halos is shown by the thin solid line.

Also note that $p(a/b|a/c) = 0$ for $a/b < \max(a/c, 0.5)$. The PDF for the concentration parameter is

$$p(c_e) = \frac{1}{\sqrt{2\pi} \times 0.3} \exp \left[-\frac{(\ln c_e - \ln \bar{c}_e)^2}{2(0.3)^2} \right] \frac{1}{c_e}. \quad (11)$$

For the median concentration parameter \bar{c}_e , we adopt a fitting formula given by JS02 (see also OLS03):

$$\bar{c}_e = 1.35 \exp \left[-\left\{ \frac{0.3}{(a/c)(M_{\text{vir}}/M_*)^{0.07[\Omega(z)]^{0.7}}} \right\}^2 \right] \times A_e \sqrt{\frac{\Delta_{\text{vir}}(z_c)}{\Delta_{\text{vir}}(z)}} \left(\frac{1+z_c}{1+z} \right)^{3/2}, \quad (12)$$

with z_c being the collapse redshift of the halo of mass M_{vir} and $A_e = 1.1$ in the Lambda-dominated CDM model (JS02). For spherical halos, large-separation lens statistics are highly sensitive to the concentration distribution (both the median and the scatter; see Kuhlen et al. 2004). However, we checked that in the triaxial model the sensitivity is much reduced because there is such a broad distribution of axis ratios; hence we do not present results with a different median or scatter in the concentration distribution. Finally, the PDFs for the orientation angles are

$$p(\theta) = \frac{\sin \theta}{2}, \quad (13)$$

$$p(\phi) = \frac{1}{2\pi}, \quad (14)$$

corresponding to random 3-d orientations.

3. LENSING PROBABILITIES AND IMAGE MULTIPLICITIES IN THE TRIAXIAL HALO MODEL

3.1. Dependence of the triaxiality

We begin by examining how the lensing probabilities and image multiplicities vary when we change the degree of triaxiality. We remove the integral over a/c in equation (7) to compute the lensing probabilities at fixed

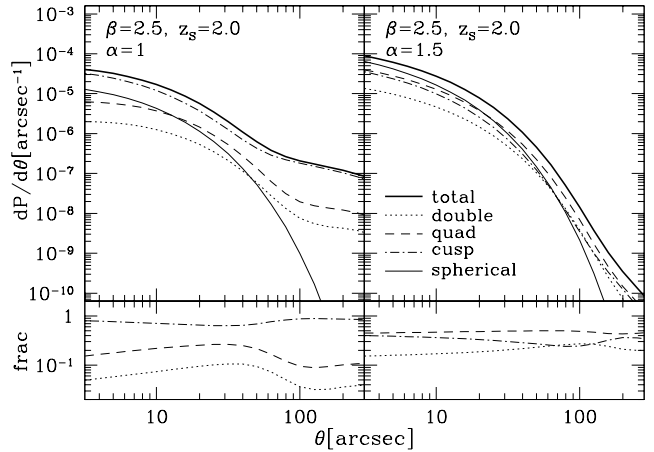


FIG. 5.— Lensing probabilities and image multiplicities with triaxial dark halos as a function of image separation θ . The source is placed at $z_s = 2.0$, and slope of the source luminosity function is fixed to $\beta = 2.5$.

triaxiality (we still integrate over the intermediate axis ratio a/b and over random orientations). We can then plot the probabilities as a function of a/c , as shown in Figure 4. In this example, we place the source at redshift $z_s = 2.0$, and we use a source luminosity function with slope $\beta = 2.5$. We compute the probabilities for an image separation of $\theta = 15''$, similar to that of the one known large-separation lensed quasar SDSS J1004+4112 (Inada et al. 2003).

For $a/c \rightarrow 1$ we recover the spherical case. As a/c decreases (the triaxiality increases), at first the total lensing probability stays roughly constant but the fraction of quadruples rises; this is similar to the effects of ellipticity on isothermal lenses (see Keeton et al. 1997; Rusin & Tegmark 2001). Then the probability for naked cusp image configurations begins to rise dramatically, and they come to dominate the total probability. Interestingly, the sum of the probabilities for quadruple and double lenses is roughly equal to the probability for spherical halos for most values of a/c , at least for this example with image separation $\theta = 15''$ (also see Figures 5–7 below). This suggests that the enhancement in the total lensing probability is mainly driven by naked cusp configurations. The $\alpha = 1$ and 1.5 cases both have these qualitative features, and they differ only in the quantitative details. Since the typical triaxiality in CDM simulations is $a/c \sim 0.5$ (JS02), it appears that triaxiality can have a significant effect on the statistics of large-separation lenses.

3.2. Full results

To compute the full impact of triaxiality on lens statistics, we must integrate over an appropriate triaxiality distribution (as in equation 7). Figure 5 shows the resulting lensing probabilities and image multiplicities as a function of the image separation θ . Again, we place the source quasar at $z_s = 2.0$, and fix the slope of the source luminosity function to $\beta = 2.5$. The first important result is that the triaxial model predicts larger lensing probabilities than the spherical model for all image separations. The enhancement is a factor of ~ 4 for $\alpha = 1$, and a factor of ~ 2 for $\alpha = 1.5$, if the image separation is not so large ($\theta \lesssim 30''$). At larger separations

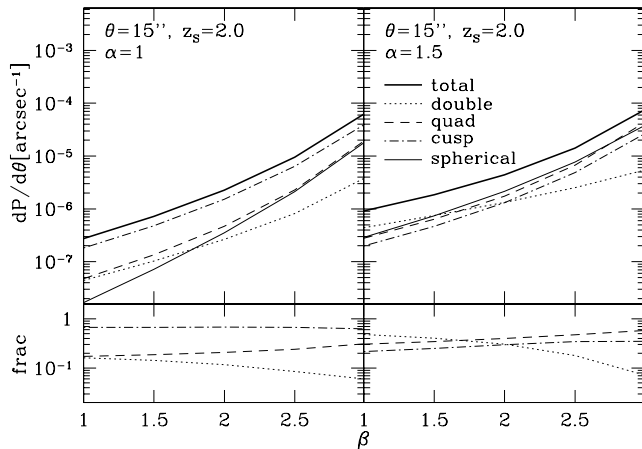


FIG. 6.— Lensing probabilities and image multiplicities with triaxial dark halos as a function of the slope of the source luminosity function β . We consider an image separation of $\theta = 15''$, and we place the source at $z_s = 2.0$.

it seems that the effect of triaxiality is even more significant, especially for $\alpha = 1$; we will discuss this issue in §3.3.

There are several interesting results in the image multiplicities. The $\alpha = 1$ and 1.5 cases have very different multiplicities: with $\alpha = 1$ the lensing probability is dominated by cusp configurations; while with $\alpha = 1.5$ quadruple lenses are somewhat more common than cusps. Neither result is very sensitive to the image separation. In both cases double lenses are fairly uncommon, which is very different from the situation with normal arcsecond-scale lenses produced by nearly-isothermal galaxies. This result is consistent with previous theoretical conclusions that image multiplicities depend on the central concentration of the lens mass distribution, such that less concentrated profiles tend to produce more quadruple and cusp lenses (Kassiola & Kovner 1993; Kormann, Schneider, & Bartelmann 1994; Rusin & Tegmark 2001; Evans & Hunter 2002; Dalal et al. 2004). The important point for observations is that if dark halos have inner profiles with $\alpha \lesssim 1.5$, then many or even most large-separation lenses should be quadruples or cusps rather than doubles. (We will consider the implications for SDSS J1004+4112 in §4.) Another point is that the image multiplicities are sensitive to the inner density profile, so they offer a new method for probing dark matter density profiles that is qualitatively different from methods discussed before.

Magnification bias is important in lens statistics, particularly in image multiplicities, because it gives more weight to quadruple and cusp configurations (which tend to have large magnifications) than to doubles. We should therefore understand what happens when we modify the magnification bias by varying the slope β of the source luminosity function. The results are shown in Figure 6 (for image separation $\theta = 15''$ and source redshift $z_s = 2.0$). The lensing probabilities increase as β increases, because as the source luminosity function becomes steeper magnification bias becomes stronger.⁶ Interestingly, the increase in the total probability due to triaxiality weakens

⁶ Note that the magnification bias diverges if the luminosity function is a pure power law with $\beta \geq 3$, so we are restricted to shallower cases.

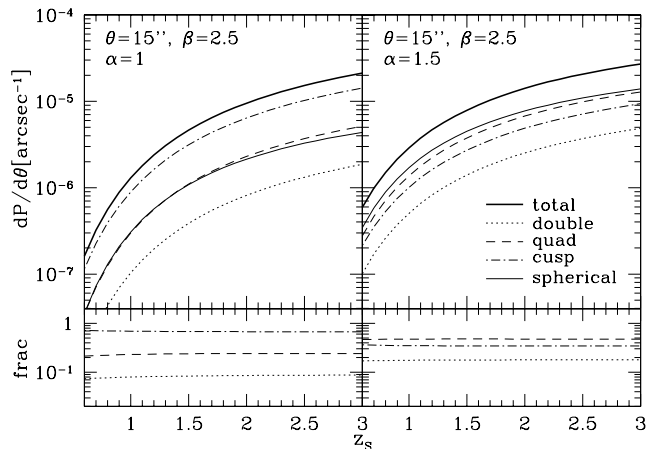


FIG. 7.— Lensing probabilities and image multiplicities as a function of source redshift z_s . We fix the image separation to $\theta = 15''$ and the of the source luminosity function to $\beta = 2.5$.

as β increases, although the effect is not strong. As for the image multiplicities, $\alpha = 1$ halos are always dominated by cusp lenses, although for sufficiently steep luminosity functions quadruples become fairly common. With $\alpha = 1.5$ halos, when magnification bias is weak ($\beta \sim 1$) doubles are the most probable, but as magnification bias strengthens (β increases) quadruples receive more weight and become the most likely. In practice, the effective values of β are larger than ~ 1.5 for both optical (e.g., Boyle et al. 2000) and radio surveys (e.g., Rusin & Tegmark 2001), so we expect cusps to dominate for $\alpha = 1$ and quadruples to be the most common for $\alpha = 1.5$.

Finally, we consider whether the results depend on the source redshift, as shown in Figure 7. The lensing probabilities rise with z_s , because there is more volume and hence more deflectors between the observer and the source. In addition, geometric effects mean that a given halo can produce a larger image separation when the source is more distant, so the halo mass required to produce a given image separation goes down and the abundance of relevant deflectors goes up. However, the probability increase affects the different image configurations in basically the same way, so the image multiplicities are quite insensitive to the source redshift. Therefore, we conclude that details of the source redshift distribution are not so important for image multiplicities, at least when the source luminosity function has a power law shape.

3.3. Statistics at larger image separations

In Figure 5, at very large image separations ($\theta \gtrsim 100''$) the lensing probabilities in the triaxial halo model are orders of magnitude larger than those in the spherical halo model. In addition, at these very large separations the $\alpha = 1$ case produces higher probabilities than the more concentrated $\alpha = 1.5$ case. Both features are puzzling and invite careful consideration.

Figure 8 shows the dependence of total lensing probability on the lower limit of the integral over a/c . In the previous calculations, we assumed $(a/c)_{\min} = 0.1$. This figure shows that for $\theta = 15''$ the results are quite insensitive to $(a/c)_{\min}$, suggesting that the contribution from extremely triaxial halos is negligible. For $\theta = 200''$, how-

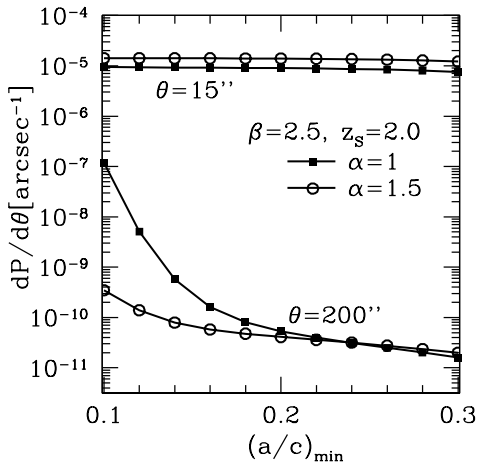


FIG. 8.— Dependence of the lensing probability on the cutoff in a/c . Both $\theta = 15''$ and $200''$ are shown. Filled squares and open circles denote $\alpha = 1$ and 1.5 , respectively. The slope of the luminosity function is fixed to $\beta = 2.5$.

ever, the lensing probability rapidly decreases as $(a/c)_{\min}$ increases. In other words, the lensing probability at very large image separations seems to be dominated by very small a/c , or very large triaxialities.

Results that are dominated by such extreme halos are probably not very reliable. They depend sensitively on both the assumed PDF for the axis ratio a/c (eq. [9]) and the correlation between a/c and the concentration c_e (eq. [12]) at very small axis ratios. The fitting forms presented by JS02 were intended to reproduce the PDF and correlation at $a/c \gtrsim 0.3$, and it is unclear whether they are still accurate at $a/c \sim 0.1$. In addition, even if we know accurate fitting forms, such a situation implies that sample variance (i.e., the effect of the finite number of lensing clusters) may be quite large.

Another ambiguity is the projection effect. In this paper, we assumed that the density profile (eq. [2]) extends beyond the virial radius, and in projecting along the line of sight we integrated the profile to infinity. Although it is not clear whether we should cut off the profile at the virial radius or not (e.g., Takada & Jain 2003), the effect of the extended profile on the gravitational lensing is not so large for normal dark halos. However, when a/c is small enough, equation (12) indicates that the concentration parameter c_e becomes smaller than unity, so the effect of the extended profile outside the virial radius is quite significant. The puzzling feature that the $\alpha = 1$ case produces higher probabilities than the $\alpha = 1.5$ case at very large separations can be ascribed to the projection effect, because the effect is more significant for shallower density profiles.

Thus, lenses with extremely large image separations are associated with the most extreme dark matter halos, and it may be difficult to make reliable predictions about them. We emphasize, though, that these issues do not apply to lenses with separations $\theta \lesssim 30''$, and on these scales we believe our results to be robust.

4. PREDICTIONS FOR THE SDSS

In the previous section, we assumed a simple power law source luminosity function to understand the general effects of triaxiality. Here we consider a specific luminosity

function appropriate for quasars, and further customize our predictions to quasars in the Sloan Digital Sky Survey.

We adopt the double power law B -band luminosity function for quasars proposed by Boyle, Shanks, & Peterson (1988),

$$\phi_L(z_S, L)dL = \frac{\phi_*}{[L/L_*(z_S)]^{\beta_l} + [L/L_*(z_S)]^{\beta_h}} \frac{dL}{L_*(z_S)}, \quad (15)$$

and use $\beta_h = 3.43$ and $\beta_l = 1.64$ (see Boyle et al. 2000). We let the break luminosity evolve following a model that reproduces the low-redshift luminosity function as well as the space density of high-redshift quasars (see Wyithe & Loeb 2002; Oguri et al. 2004). In practice we actually use the cumulative luminosity function

$$\Phi_L(z_S, L) = \int_L^\infty \phi_L(z_S, L)dL, \quad (16)$$

to calculate the biased cross section (see §2.2)

$$B\bar{\sigma} = \int dX dY \frac{\Phi_L(L/\mu)}{\Phi_L(L)}. \quad (17)$$

We approximate that the SDSS quasar sample is a sample with a flux limit of $i^* = 19.7$.⁷ One needs a cross-filter K -correction to convert observed i^* magnitudes to absolute B -band luminosity. We adopt the following form

$$K_{Bi}(z) = -2.5(1 - \alpha_s) \log(1 + z) - 2.5\alpha_s \log\left(\frac{7500}{4400}\right) - 0.12, \quad (18)$$

with $\alpha_s = 0.5$ (Oguri et al. 2004). Finally, we approximate the redshift distribution (see Fig. 1 of Oguri et al. 2004) with the following Gaussian distribution:

$$p(z_S)dz_S = \frac{1}{1.21} \exp\left\{-\frac{(z - 1.45)^2}{2(0.55)^2}\right\} dz_S \quad (0.6 < z_S < 2.3). \quad (19)$$

We have confirmed that the results using these approximations agree well with those obtained by fully taking account of the observed redshift and magnitude distributions.

Figure 9 shows the lensing probabilities and image multiplicities as a function of image separation θ for the SDSS quasar sample. Again large-separation lenses are dominated by cusp configurations for $\alpha = 1$, but all three configurations are almost equally likely for $\alpha = 1.5$. Therefore, we confirm that image multiplicities in SDSS large-separation lenses will offer interesting information on the density profile of dark halos. We can now consider whether it is statistically natural that the first large-separation lens in the SDSS is a quadruple lens. We find that for an image separation $\theta = 15''$ the fractions of quadruple lenses are ~ 0.2 and ~ 0.4 for $\alpha = 1$ and 1.5 , respectively. Thus $\alpha = 1.5$ could explain the discovery of the quadruple lens somewhat better, but $\alpha = 1$ is also not unnatural.

⁷ The SDSS quasar target selection is aimed to choose quasars with $i^* \lesssim 19.1$ (Richards et al. 2002). However, we assume a flux limit of $i^* = 19.7$ because there are quasars with $i^* > 19.1$ in the SDSS quasar sample which are, for example, first targeted as different objects but revealed to be quasars.

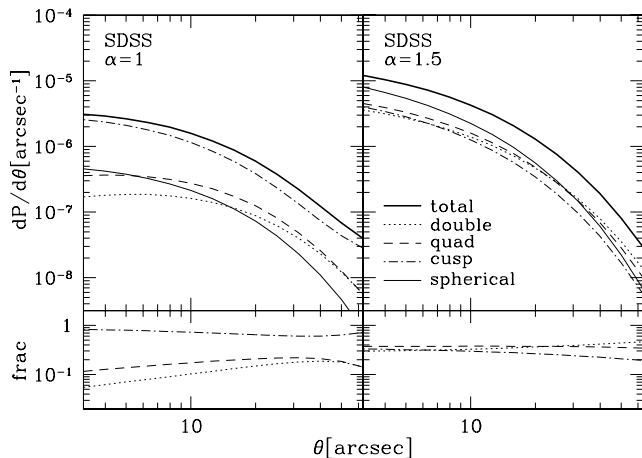


FIG. 9.— Lensing probabilities and image multiplicities for SDSS quasars at redshifts $0.6 < z_S < 2.3$.

Finally, we can use the discovery of SDSS J1004+4112, together with the lack of large-separation lenses in the Cosmic Lens All-Sky Survey (CLASS; Phillips et al. 2001), to constrain the cosmological parameter σ_8 describing the normalization of the density fluctuation power spectrum. Using spherical models, Oguri et al. (2004) found that the discovery of SDSS J1004+4112 required rather large values of either α or σ_8 , but given the importance of triaxiality we should revisit this question. For the SDSS, we compute the expected number of large-separation lenses with $7'' < \theta < 60''$ among the 29811 SDSS quasars. For CLASS, we adopt a power law source luminosity function with $\beta = 2.1$ (see Rusin & Tegmark 2001), fix the source redshift to $z_S = 1.3$ (see Marlow et al. 2000), and calculate the expected number of lenses with $6'' < \theta < 15''$ among 9284 flat-spectrum radio sources (Phillips et al. 2001). We then compute the likelihood

$$\mathcal{L} \propto (1 - e^{-N_{\text{SDSS}}}) e^{-N_{\text{CLASS}}}, \quad (20)$$

which represents the Poisson probability of observing no large-separation lenses in CLASS when N_{CLASS} are expected, and at least one large-separation lens in SDSS when N_{SDSS} are expected. (There may be other large-separation lenses in the SDSS sample that have not yet been identified.) We consider two possibilities for the expected number of lenses in the SDSS: (1) the total number of lenses N_{tot} is used as N_{SDSS} ; (2) only the number of quadruple lenses N_{quad} is because the discovered lens is quadruple.

Figure 10 shows the resulting maximum likelihood constraints on σ_8 . We find that $\sigma_8 \sim 1$ explains the data well, although the details depend on the value of α and the choice of N_{SDSS} . Only the case with $\alpha = 1$ and $N_{\text{SDSS}} = N_{\text{quad}}$ prefers relatively large σ_8 , but $\sigma_8 = 1$ is still allowed at the 2σ level. At present the data do not allow particularly strong constraints on σ_8 . Nevertheless, we can conclude that the status large-separation lenses is quite consistent with the predictions of CDM given $\sigma_8 \sim 1$.

For comparison, Figure 10 also shows results for spherical halos. It turns out that the spherical model overestimates the value of σ_8 by ~ 0.1 for $\alpha = 1$ and ~ 0.2 for $\alpha = 1.5$, compared with cases where we take $N_{\text{SDSS}} =$

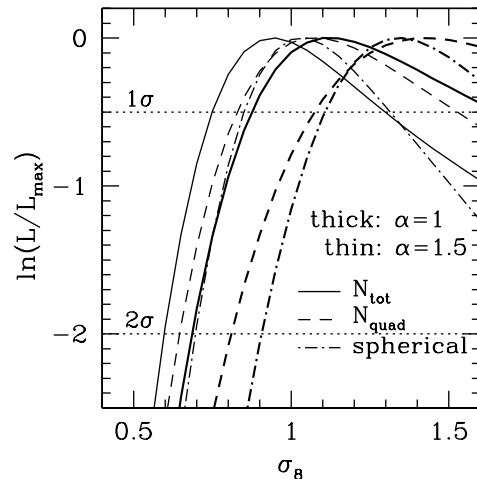


FIG. 10.— Maximum likelihood estimates for σ_8 from combining the discovery of SDSS J1004+4112 in SDSS with the lack of large-separation lenses in CLASS. In making predictions for SDSS, we consider two cases: the appropriate prediction could be the total number of lenses (solid lines); or since SDSS J1004+4112 is a quad the appropriate quantity could be the number of quadruples (dashed lines). The likelihoods for $\alpha = 1$ and 1.5 are shown by thick and thin lines, respectively. Results for spherical halos are also shown by dash-dotted lines for reference.

N_{tot} . Triaxiality is therefore an important systematic effect in these cases. Interestingly, the best-fit values of σ_8 from spherical models are quite similar to those from triaxial models with $N_{\text{SDSS}} = N_{\text{quad}}$. In both cases, the likelihood function for the spherical model is narrower than for the triaxial model, indicating that the spherical model would underestimate the statistical uncertainties in σ_8 .

5. SUMMARY AND DISCUSSION

The dark matter halos predicted by the CDM model are triaxial rather than spherical, which has a significant effect on the statistics of large-separation gravitational lenses. Triaxiality systematically enhances the lensing probability by a factor of ~ 4 if dark halos have an inner density profile with $\alpha = 1$, or a factor of ~ 2 if $\alpha = 1.5$. The effects may be even more dramatic at very large image separations ($\theta \gtrsim 100''$), although such lenses are very sensitive to the most triaxial halos and so the predictions are not as reliable. Thus, triaxiality must be added to the list of important systematic effects that need to be included in calculations of large-separation lens statistics. (Some of the other effects are the inner density profile and the shape of the distribution of concentration parameters, as found by previous studies of large-separation lens statistics using spherical halos.)

Triaxial modeling allows us to predict the image multiplicities for large-separation lenses. We found that the multiplicities depend strongly on the density profile: for $\alpha = 1$, lenses are dominated by naked cusp image configurations; while for $\alpha = 1.5$, quadruple configurations are the most probable. Double lenses, which are dominant among normal arcsecond-scale lenses, are subdominant in both cases. Note that cusp lenses can be distinguished from doubles by the presence of a third image comparable in brightness to the other two, and by the configuration of image positions. The differences can be

scribed to the different mass density profiles, and they indicate that the multiplicities of large-separation lenses will provide a qualitatively new probe of the central density profiles of massive dark matter halos (and hence a new test of CDM).

We have computed lensing probabilities and image multiplicities for the SDSS quasar sample. We predict that for both $\alpha = 1$ and 1.5 most of the large-separation lenses should be quadruples or cusps. The fractions of quadruple lenses at separations of $\theta = 15''$ are ~ 0.2 and ~ 0.4 for $\alpha = 1$ and 1.5, respectively. Thus it is not surprising that the first large-separation lens discovered is a quadruple. In addition, we computed the expected number of large-separation lenses in both SDSS and CLASS, and found that the data are consistent with the CDM model with $\sigma_8 \sim 1$, in agreement with other measurements (e.g., Spergel et al. 2003, and references therein). Thus, the discovery of SDSS J1004+4112 can be interpreted as additional support for CDM on non-linear cluster scales.

The prediction that triaxial halos produce significant fractions of quadruple and cusp lenses should be kept in mind when considering samples of candidate large-separation lenses. For example, Miller et al. (2004) found six large-separation double lens candidates in the 2dF Quasar Redshift Survey, but no quadruple or cusp lens candidates. Even accounting for small number statistics, our results suggest that such a high fraction of doubles would be inconsistent with CDM at more than 3σ ,⁸ and that it would be surprising if many of the six candidates are genuine lens systems.

We note that the triaxial dark halo model we adopted in this paper can be improved in several ways. First, we assumed that the axis ratios of the triaxial ellipsoids are constant with radius. However, JS02 showed that the axis ratios decrease slightly toward the halo centers: a/c decreases by ~ 0.2 as the mean radius decreases from $\sim 0.6r_{\text{vir}}$ to $\sim 0.06r_{\text{vir}}$. Since strong lensing is most sensitive to the inner parts of dark halos, it is possible that we have actually underestimated the effects of triaxiality on the statistics of large-separation lenses. On the other hand, including baryons (which were neglected in the simulations of JS02) would tend to make dark halos rounder by $\Delta(a/c) \sim 0.1\text{--}0.2$ because of the isotropic gas

pressure.

While our theoretical model is much more realistic than the simple spherical model, we have still made several simplifying assumptions. One is that we have neglected substructure in dark halos. The galaxies in massive cluster halos do not have a large effect on the statistics of lensed arcs (Meneghetti et al. 2000), but it is not obvious whether or not they would affect large-separation lenses. Substructure can affect the image multiplicities for isothermal lenses (Cohn & Kochanek 2004), so it should be considered for CDM halos as well. Another effect we have neglected is the presence of a massive central galaxy in a cluster. Meneghetti, Bartelmann, & Moscardini (2003b) claim that central galaxies do not have a large effect on arc statistics. However, because our results depend on the inner slope of the density profile, and a central galaxy effectively increases the concentration, this effect should be considered. A third phenomenon we have neglected is cluster merger events. Indeed, mergers can change the shapes of critical curves and caustics substantially, and thus have a great impact on lensing cross sections (Torri et al. 2004). To estimate the effect on large-separation lens statistics, we would need a realistic model of the cluster merger event rate and the physical conditions of merger events. Addressing these various issues to improve the accuracy of the theoretical predictions is beyond the scope of this paper, but is certainly of interest for future work.

We thank Y. P. Jing, Jounghun Lee, Yasushi Suto, Masahiro Takada, Naohisa Inada, and Andrey Kravtsov for discussions. MO is supported in part by JSPS through JSPS Research Fellowship for Young Scientists. CRK is supported by NASA through Hubble Fellowship grant HST-HF-01141.01-A from the Space Telescope Science Institute, which is operated by the Association of Universities for Research in Astronomy, Inc., under NASA contract NAS5-26555.

⁸ If the predicted double fraction is f_2 , then the Poisson probability of having N doubles and no quadruples or cusps is $\mathcal{L}(f_2) \propto (f_2)^N$.

REFERENCES

- Bartelmann, M. 1996, *A&A*, 313, 697
 Bartelmann, M., Huss, A., Colberg, J. M., Jenkins, A., & Pearce, F. R. 1998, *A&A*, 330, 1
 Boyle, B. J., Shanks, T., & Peterson, B. A. 1988, *MNRAS*, 235, 935
 Boyle, B. J., Shanks, T., Croom, S. M., Smith, R. J., Miller, L., Loaring, N., & Heymans, C. 2000, *MNRAS*, 317, 1014
 Chae, K.-H. 2003, *MNRAS*, 346, 746
 Chen, D. 2004, *A&A*, 418, 387
 Cohn, J. D., & Kochanek, C. S. 2004, *ApJ*, in press (astro-ph/0306171)
 Dalal, N., Holder, G., & Hennawi, J. 2004, *ApJ*, in press (astro-ph/0310306)
 Evans, N. W., & Hunter, C. 2002, *ApJ*, 575, 68
 Fukushige, T., & Makino, J. 1997, *ApJ*, 477, L9
 Fukushige, T., Kawai, A., & Makino, J. 2004, *ApJ*, in press (astro-ph/0306203)
 Gladders, M. D., Hoekstra, H., Yee, H. K. C., Hall, P. B., & Barrientos, L. F. 2003, *ApJ*, 593, 48
 Huterer, D., & Ma, C. 2004, *ApJ*, 600, L7
 Huterer, D., & Keeton, C. R. 2004, in preparation
 Inada, N., et al. 2003, *Nature*, 426, 810
 Jenkins, A., Frenk, C. S., White, S. D. M., Colberg, J. M., Cole, S., Evrard, A. E., Couchman, H. M. P., & Yoshida, N. 2001, *MNRAS*, 321, 372
 Jing, Y. P., & Suto, Y. 2000, *ApJ*, 529, L69
 Jing, Y. P., & Suto, Y. 2002, *ApJ*, 574, 538 (JS02)
 Kassiola, A., & Kovner, I. 1993, *ApJ*, 417, 450
 Keeton, C. R. 2001a, *ApJ*, 561, 46
 Keeton, C. R. 2001b, preprint (astro-ph/0102341)
 Keeton, C. R., Kochanek, C. S., & Seljak, U. 1997, *ApJ*, 482, 604
 Keeton, C. R., & Madau, P. 2001, *ApJ*, 549, L25
 Kuhlen, M., Keeton, C. R., & Madau, P. 2004, *ApJ*, 601, 104
 Kochanek, C. S. 1995, *ApJ*, 453, 545
 Kochanek, C. S. 1996, *ApJ*, 466, 638
 Kormann, R., Schneider, P., & Bartelmann, M. 1994, *A&A*, 284, 285
 Lewis, G. F., Carilli, C., Papadopoulos, P., & Ivison, R. J. 2002, *MNRAS*, 330, L15
 Li, L. X., & Ostriker, J. P. 2002, *ApJ*, 566, 652
 Lopes, A. M., & Miller, L. 2004, *MNRAS*, 348, 519
 Luppino, G. A., Gioia, I. M., Hammer, F., Le Fèvre, O., & Annis, J. A. 1999, *A&AS*, 136, 117
 Lynds, R., & Petrosian, V. 1986, *BAAS*, 18, 1014
 Macciò, A. V. 2004, *MNRAS*, submitted (astro-ph/0402657)
 Maoz, D., Rix, H.-W., Gal-Yam, A., Gould, A. 1997, *ApJ*, 486, 75

- Marlow, D. R., Rusin, D., Jackson, N., Wilkinson, P. N., & Browne, I. W. A. 2000, *AJ*, 119, 2629
- Meneghetti, M., Bolzonella, M., Bartelmann, M., Moscardini, L., & Tormen, G. 2000, *MNRAS*, 314, 338
- Meneghetti, M., Yoshida, N., Bartelmann, M., Moscardini, L., Springel, V., Tormen, G., & White S. D. M. 2001, *MNRAS*, 325, 435
- Meneghetti, M., Bartelmann, M., & Moscardini, L. 2003a, *MNRAS*, 340, 105
- Meneghetti, M., Bartelmann, M., & Moscardini, L. 2003b, *MNRAS*, 346, 67
- Miller, L., Lopes, A. M., Smith, R. J., Croom, S. M., Boyle, B. J., Shanks, T., & Outram, P. 2004, *MNRAS*, 348, 395
- Molikawa, K., & Hattori, M. 2001, *ApJ*, 559, 544
- Moore, B., Quinn, T., Governato, F., Stadel, J., & Lake, G. 1999, *MNRAS*, 310, 1147
- Mortlock, D. J., & Webster, R. L. 2000, *MNRAS*, 319, 872
- Nakamura, T. T., & Suto, Y. 1997, *Prog. Theor. Phys.*, 97, 49
- Narayan, R., & White, S. D. M. 1988, *MNRAS*, 231, 97P
- Navarro, J. F., Frenk, C. S., & White, S. D. M. 1997, *ApJ*, 490, 493
- Ofek, E. O., Maoz, D., Prada, F., Kolatt, T., & Rix, H.-W. 2001, *MNRAS*, 324, 463
- Oguri, M. 2002, *ApJ*, 580, 2
- Oguri, M. 2003, *MNRAS*, 339, L23
- Oguri, M., Lee, J., & Suto, Y. 2003, *ApJ*, 599, 7 (OLS03)
- Oguri, M., Taruya, A., & Suto, Y. 2001, *ApJ*, 559, 572
- Oguri, M., Taruya, A., Suto, Y., & Turner, E. L. 2002, *ApJ*, 568, 488
- Oguri, M., et al. 2004, *ApJ*, 605, 78
- Phillips, P. M., et al. 2001, *MNRAS*, 328, 1001
- Power, C., Navarro, J. F., Jenkins, A., Frenk, C. S., White, S. D. M., Springel, V., Stadel, J., & Quinn, T. 2002, *MNRAS*, 338, 14
- Richards, G. T., et al. 2002, *AJ*, 123, 2945
- Rusin, D. 2002, *ApJ*, 572, 705
- Rusin, D., & Tegmark, M. 2001, *ApJ*, 553, 709
- Sarbu, N., Rusin, D., & Ma, C.-P. 2001, *ApJ*, 561, L147
- Schramm, T. 1990, *A&A*, 231, 19
- Soucail, G., Fort, B., Mellier, Y., & Picat, J. P. 1987, *A&A*, 172, L14
- Spergel, D. N., et al. 2003, *ApJS*, 148, 175
- Takada, M., & Jain, B. 2003, *MNRAS*, 344, 857
- Takahashi, R., & Chiba, T. 2001, *ApJ*, 563, 489
- Torri, E., Meneghetti, M., Bartelmann, M., Moscardini, L., Rasia, E., & Tormen, G. 2004, *MNRAS*, 349, 476
- Wambsganss, J., Bode, P., & Ostriker, J. P. 2004, *ApJ*, in press (astro-ph/0306088)
- Wambsganss, J., Cen, R., Ostriker, J. P., & Turner, E. L. 1995, *Science*, 268, 274
- Wyithe, J. S. B., & Loeb, A. 2002, *ApJ*, 577, 57
- Wyithe, J. S. B., Turner, E. L., & Spergel, D. N. 2001, *ApJ*, 555, 504
- Zaritsky, D., & Gonzalez, A. H. 2003, *ApJ*, 584, 691
- Zhao, H. 1996, *MNRAS*, 278, 488